Thermal and structural analysis of W-7X first wall graphite tiles under direct NBI loads

Vojtěch Smolík [a,b,*], Mikhail Khokhlov [b], Axel Lorenz [b], Samuel Lazerson [c,b], Victor Bykov [b], Paul McNeely [b], W7-X team [b,1]

[a] Czech Technical University in Prague, Czech Republic
[b] Max Planck-Institut für Plasmaphysik, Greifswald, Germany
[c] Gauss Fusion GmbH, Garching bei München, Germany

Keywords:
Thermal and structural analysis
Wendelstein 7-x
ANSYS mechanical
Graphite tile
NBI load

A B S T R A C T

Thermo-mechanical analysis of the Wendelstein 7-X neutral beam dump is presented focusing on failure phenomena resulting from strong impulsive thermal loading of the graphite tiles. One of the plasma heating systems of the Wendelstein 7-X stellarator is Neutral Beam Injection (NBI). There are two NBI boxes with currently a total injected hydrogen beam power of 7 MW and a pulse length up to 5 s. Each NBI box can be operated with four positive ion neutral injectors (PINI). A total of three PINIs were used simultaneously in the last operation campaign in 2022. NBI is highly important for the W7-X physics program, thus increasing NBI power is planned in the next operation phase. A portion of the NBI power passes through the plasma, creating a region of the first wall (FW) with a significantly increased heat load. This region, called the beam dump, could be a limiting factor for the NBI pulse length and thus it requires a precise remodeling of all constituents before the 2024/2025 operation phases to prevent repeated structural damage to this area. Since the graphite tiles are attached by multiple bolts to the CuCrZr heat sinks, the thermal expansion of graphite can induce significant stress in the graphite. The safety limiting factor is the induced thermal stress in the graphite tile due to the NBI beam power load. ANSYS Mechanical model was developed, including the bolted connections, and analyzed to examine the effect of the heat load on the FW components and to evaluate the maximal allowed duration of the NBI beam. A coupled transient simulation of the thermal and structural analysis is performed. The calculation used the NBI heat loads on the FW surfaces estimated by the BEAMS3D code. This paper presents the results of the numerical analysis and the related operating limits.

1. Introduction

One of the plasma heating systems of the Wendelstein 7-X stellarator (W7-X) is Neutral Beam Injection (NBI). There are two NBI boxes with a total injected hydrogen beam power of 7 MW and a pulse length up to 5 s. Each NBI box can be operated with four positive ion neutral injectors (PINIs) [1]. A total of three PINIs were used simultaneously in the last operational campaign in 2022. During one of the calibration shots in the last campaign, a graphite tile on the wall opposite the NBI injector S3 was damaged. Fig. 1 shows the view through NBI port AEK20 on the beam dump and in particular on the heat shield region where the damaged tile was located in half module 20 (HM20). NBI is highly important for the W7-X physics program; thus increasing the NBI power is planned for the next operational phase, and stricter operational limits need to be set to prevent any further damage to the heat shield. This article describes the development of a FEA model of graphite tile, created to uncover the thermal and structural limits [2].

W7-X heat shields of the first wall consist of graphite tiles attached to CuCrZr heat sinks with TZM screws. The heat sinks are cooled via a water-cooled stainless steel pipe, which is connected through brazing. The heat shields are designed to withstand plasma heat load during the operation in the range up to 250 $kW{\cdot}m^{-2}$ [3]. A heat load increased above this threshold represents a significant challenge for the heat shield component. For a reference, the Electron Cyclotron Resonance Heating (ECRH) system is targeted at heat shield tiles specifically designed to withstand high heat loads. In contrast, the neutral beam injection (NBI) beams are aimed at the heat shield region with only minor design modifications — an increased graphite thickness on the tiles. The heat shield thermography (HST) serves as a safety diagnostic system to protect the CuCrZr cooling structure within the NBI beam

* Corresponding author at: Max–Planck-Institut für Plasmaphysik, Greifswald, Germany.
E-mail address: vojtech.smolik@fs.cvut.cz (V. Smolík).
[1] (Grulke et al. 2024).

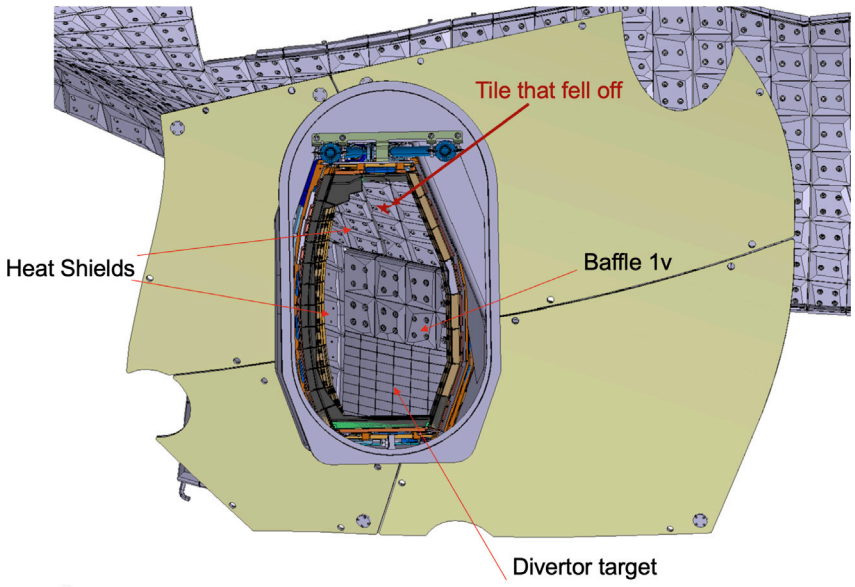

Fig. 1. View through NBI port AEK20, where the NBI source S3 is installed.

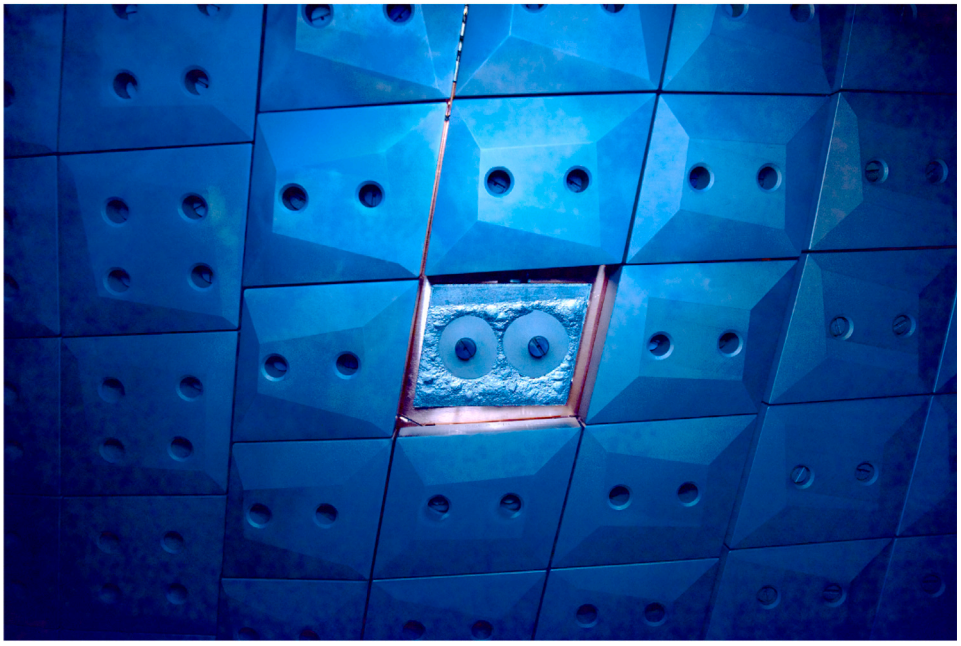

Fig. 2. The beam dump area around the damaged tile.

dump area of the W7-X vessel. A pyrometer detects when the graphite tile temperature exceeds a predefined threshold (1000 °C) and triggers beam termination. The physical temperature limit on the tile is 2000 °C but the system limits the surface temperature to 1000 °C to prevent the CuCrZr/water pipe system from being dammaged. Each NBI beam is individually monitored by a dedicated pyrometer [4] and taking into operation a new NBI source requires validation of the HTS safety function. Thus, at the end of the last operational campaign, an HST calibration NBI shot was performed with no plasma; full power was deposited on the heat shield. One of the heat shield wall tiles in the NBI beam dump area was damaged and fell off. The conical remains of graphite tile were found beneath the bolts holding the damaged tile. Remains of the graphite tile were examined in detail. Figs. 2 and 3 shows the graphite fragments, indicating the shape and dimensions of a crack that occurred.

The immediately initiated analysis had two targets to ensure safer W7-X operation: to verify the maximum duration of the NBI pulse deposited directly on the heat shields (to prevent any more damaged tiles) and the recommended dwell period between two pulses to prevent overheating of the heat shield during the operational workday.

2. The FEA models and analyses set-up

A finite element model was developed in ANSYS Mechanical 23.1, featuring graphite tiles attached by bolts to CuCrZr heat sinks. A thermal simulation of the heatup and cooldown phase is performed, followed by a structural simulation of selected timestamps. The bolted connection details, including washers and pretension state, were incorporated to reflect the physical constraints of tile expansion under thermal loading. Tile geometry is variable along the heat shield;

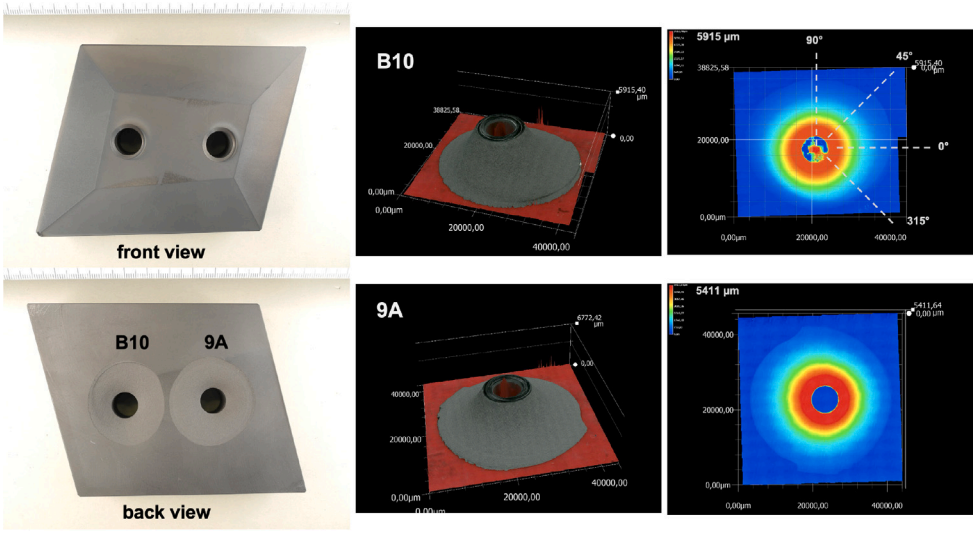

Fig. 3. The damaged graphite tile (left) and the conical remains of graphite found beneath the bolt heads measured in detail (right).

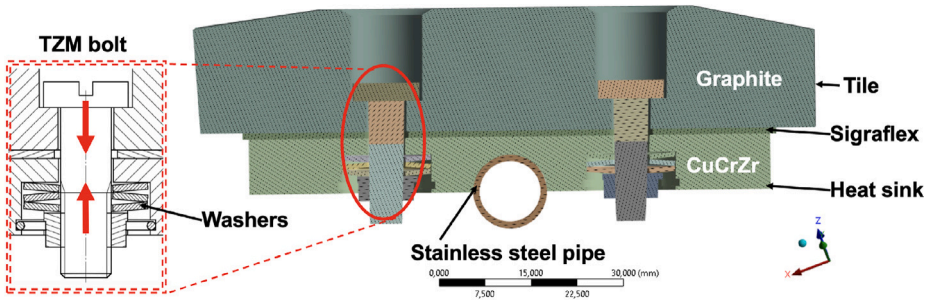

Fig. 4. Heat shield graphite tile damaged during the operation, used for the FEA simulation.

the analysis is performed on the tile that was damaged during the operation. The cross section of the tile is shown in Fig. 4.

2.1. Boundary conditions

The graphite tile (Graphite R6510) is connected to the heat sink body (CuCrZr 1.1293) using Sigraflex, a layered type of graphite with significantly anisotropic properties. Temperature dependent material properties are listed in Appendix. The thermal conductivity of Sigraflex is very low in the normal direction (through the thickness), compared to the conductivity in the plane. The heat sink is water-cooled by a stainless steel (Steel 1.4435) cooling pipe brazed to the bottom part of the CuCrZr block [5].

Two NBI sources (S3 and S4) with a nominal power of 1.8 MW per source create a beam dump area on the wall opposite the injectors. During the last campaign, the NBI was distorted upwards by the changes in magnetic field configuration, this distortion was simulated as a 0.3° shift of the NBI beam. This shift led to redistribution of the NBI load within the beam dump area. The heat flux load profile from the NBI load was estimated using the BEAMS3D code [6] for both the nominal positions of the NBI and the shifted positions. For the calibration shots without plasma, the highest average load on targeted tiles is expected to reach up to 13.5 $MW \cdot m^{-2}$ for the most exposed tile (detailed distribution in Fig. 5(b)). The BEAMS 3D code provided flux profiles that were then mapped onto the heat shield tile surfaces. The heat load used in this analysis is shown in Fig. 5(a). To estimate the model response, reduced NBI heat load can be simulated by multiplying the load profile by a constant value. Modulating the heat load can be implemented much easily than reducing the beam power in the real NBI operation.

2.2. Thermal simulation

The thermal model is set as a transient simulation: 1.5 s of NBI pulse followed by a 400 s dwell period to observe the cooldown over a long period of time between the NBI pulses. The film coefficient for 30 °C inlet temperature cooling water was set to $1.7 \cdot 10^4$ $W/m \cdot K$ [5,7]. The plasma-facing side of the graphite tile is loaded with the mapped heat flux profile; this graphite face is also included in the radiation boundary condition. The heat flux profile is shown in detail in Fig. 5(b). Radiation boundary condition of the graphite face allows it to radiate heat to ambient environment; this ambient environment with 30 °C temperature represents the cold surface of the opposite side of the W7-X chamber. Emissivity of graphite is set to 0.9, the radiation loss has a minor effect in the thermal model.

2.3. Structural simulation

Structural analysis was performed as a one-way coupled solution, where thermal results (temperature field) were transferred to evaluate the structural response under NBI heating. There are 3 major boundary conditions in the structural part of the simulation: fixed support set on one of the cooling pipe endings, bolt pretension, and the temperature profile imported to the model from the previous analysis (causing

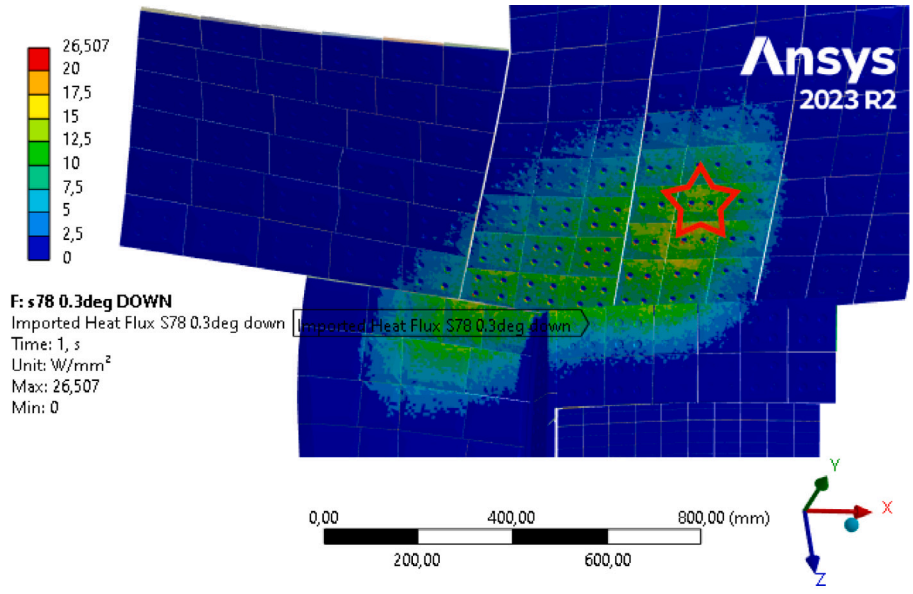

(a) The beam dump area heat load profile; the damaged tile is marked by a red star.

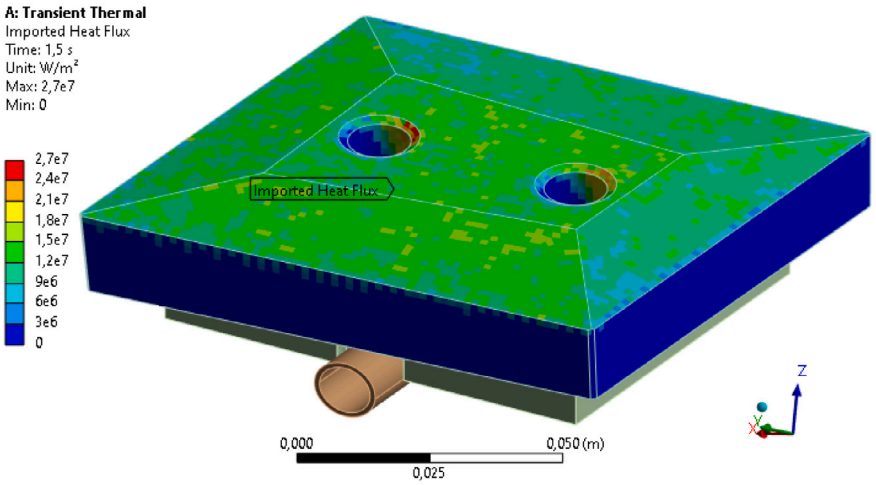

(b) Heat load mapped on the graphite tile.

Fig. 5. NBI heat flux load profile.

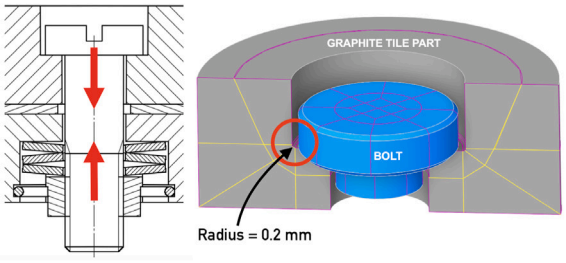

(a) Forces in the bolts and the submodel region.

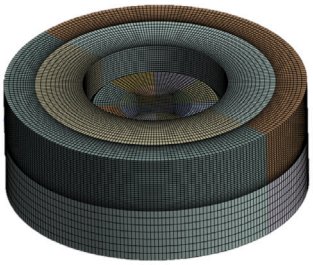

(b) Refined mesh.

Fig. 6. Local submodel structure.

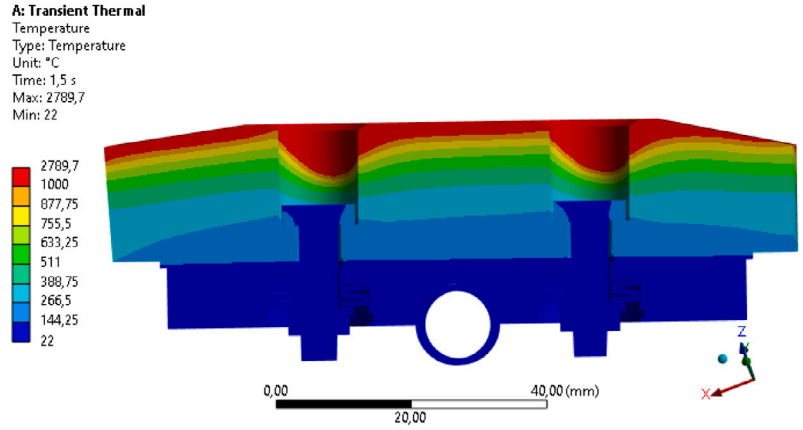

(a) Temperature profile in 1.5s of the NBI pulse.

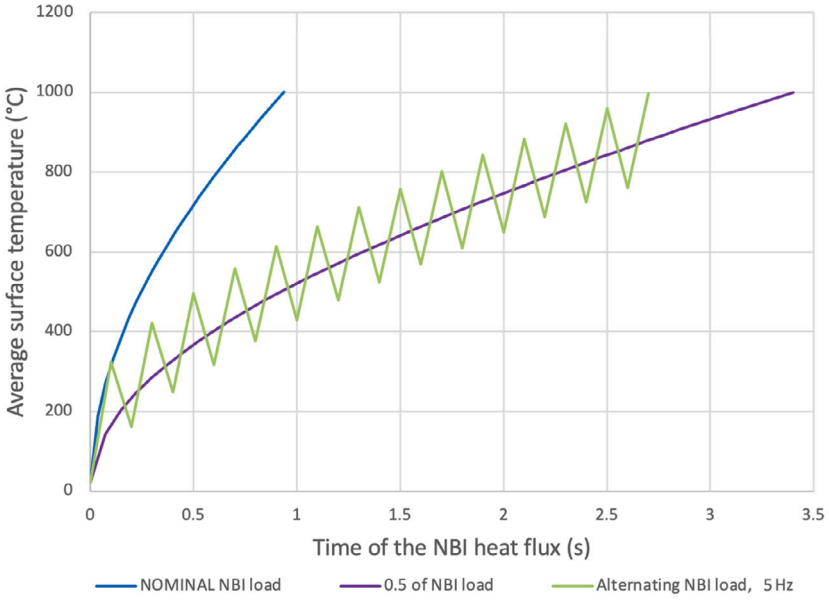

(b) Average temperature of the plasma facing graphite surface during the NBI pulse.

Fig. 7. Thermal analysis results.

the thermal expansion). According to the assembly guide, the 270° turn results in 0.75 mm displacement pretension in each bolt. This pretension leaves just 0.3 mm until the washers are fully locked. During the structural simulation, the pretension displacements in bolts are introduced in an artificial timestep of 1e-5 s, and the temperature field profile is imported afterwards in few selected time steps.

During the visual inspection, the crack propagation area was found in the graphite bolt hole corner; therefore the stresses here are in our focus. A submodel around the bolt hole was developed to focus on the stress distribution in the area of the crack initiation, introducing a bolt head chamfers and 0.2 mm radius in the graphite tile corner (based on real measurements and cutting tool dimensions). The local submodel geometry and mesh are shown in Fig. 6. Introducing the radius found in the graphite tile corner serves an important role, allowing us to calculate the exact values of stresses in this area. Without the radius, sharp corners will produce strongly mesh-dependent results in the corner area. The submodel is connected to the large structural model by importing the displacements of nodes on the submodel borders and also importing the temperature field of selected bodies. The temperature field profile affects both the thermal expansion and temperature-dependent material properties in the submodel.

3. Results

3.1. Thermal results

Temperature profiles revealed that the graphite tiles reached temperatures up to 2700 °C at the plasma facing surface within 1.5 s of nominal NBI heating load. The temperature profile with a steep temperature gradient is shown in Fig. 7(a). Edge regions around the bolt holes showed the highest thermal concentration, reaching 1000 °C within 0.5 s. This rapid heating underscores the need for dwell cooling phases to avoid temperature accumulation, thermal deformations and high stresses of the material. Fig. 7(b) shows how the maximal temperature of graphite tile evolves during the NBI pulse for the case of nominal heating power (1.8 MW per source). In attempt to decrease the

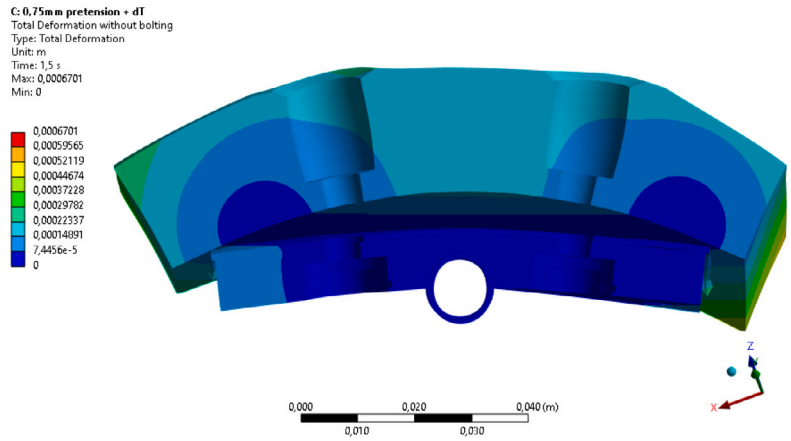

(a) Bending effect of the graphite tile.

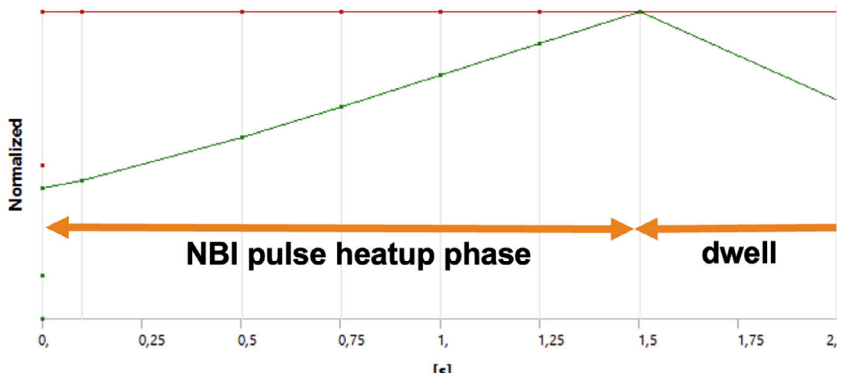

(b) Force induced in the bolts during the pretension and thermal load.

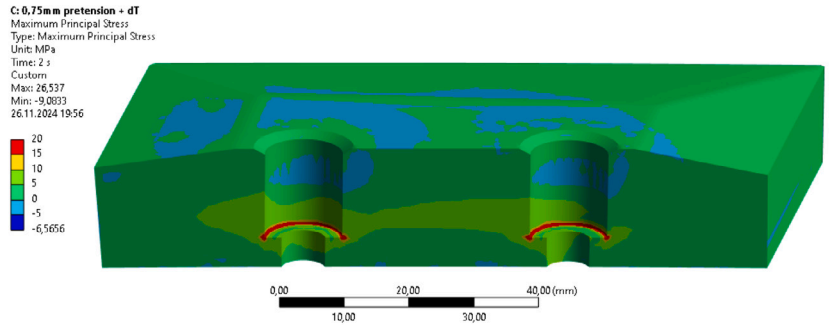

(c) Maximal principal stress in graphite body.

Fig. 8. Structural analysis results.

stresses in the tile; half of the heating power and the alternating (5 Hz modulated) loads at full power were also calculated. Average surface graphite temperature reaches 1000 °C (the HTS triggering temperature limit) after 1 s in the case of the nominal NBI load and in around 3 s for both the 5 Hz modulated load and load reduced to one half of the power. Thus, modulating the heat load results in a very similar thermal response as the load reduction.

3.2. Structural results

To evaluate the structural response to thermal load, the resulting force in the bolts is observed, shown in Fig. 8(b). The plot shows how the bolt pretension and the thermal load contribute to the force in bolts. The pretension effect on the bolt force is observed at the 1e-5 s artificial timestemp; afterwards the force in bolts is doubled during the 1.5 s of thermal load. Fig. 7(a) explains the origin of the bolt force increase. The steep temperature gradient in the graphite body induces the "bending effect" of the graphite tile, creating a gap between the graphite and the Sigraflex layer below.

This bending effect illustrated in Fig. 8(a) is a result of very high heat flux deposited over a short period of time on the plasma-facing side. Reducing or modulating the load makes the temperature distribution more even, therefore reducing the bending effect. Introducing the submodel with the corresponding corner radius in the bolt hole is necessary to evaluate the stress distribution in the area where the crack was initiated, because of the numerical stress singularity found in right-angled corners.

The secondary outcome of the bending effect is a significant reduction of thermal contact between the graphite body and the Sigraflex (heat sink). The area of thermal contact is reduced down to 10% of the initial size. This reduction of thermal contact can be neglected in simulations performed over a range of few seconds (the heat wave is

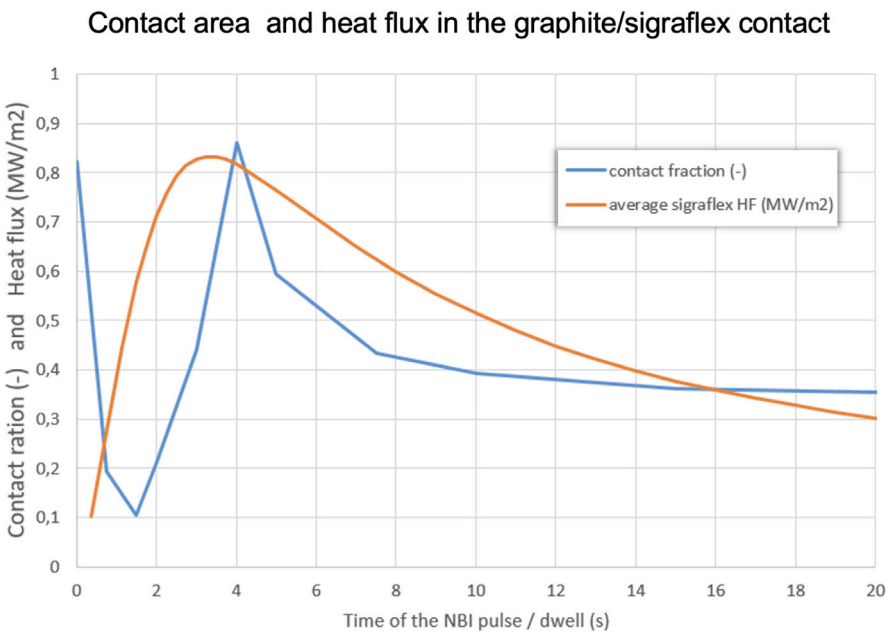

Fig. 9. Contact status between graphite and heat sink in 1 to 20 s of simulation.

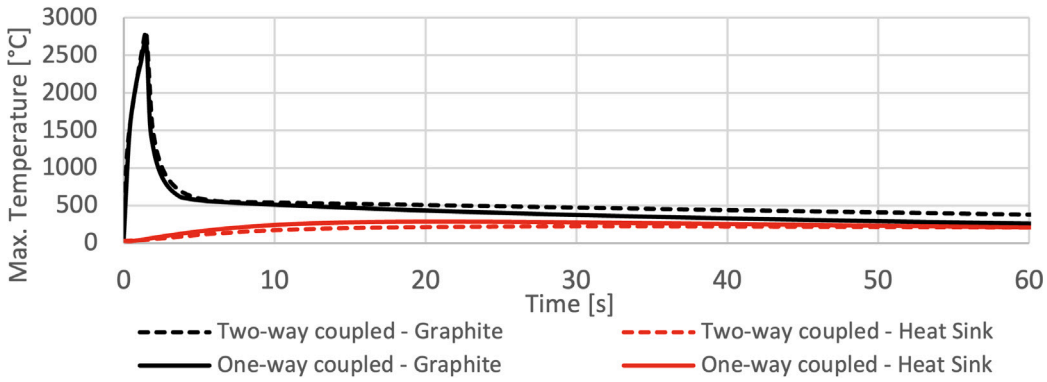

Fig. 10. Maximal heat sink and graphite temperature for 1.5 s of NBI pulse followed by a 1 min cooldown for both the one-way and two-way coupled model.

not reaching this contact significantly), but it needs to be considered for estimating the thermal response over longer pulse/dwell periods of time. Fig. 9 shows how the contact area and the average heat flux in contact evolve . We can observe the bending effect of graphite tile over the first few seconds of the simulation in Fig. 8(a). The minimal contact fraction occurs in the moment of temperature maximum around 1.5 of the NBI pulse. Afterwards, the temperature distribution is more even, suppressing the bending effect and joining the contact to the initial state at 4 s. Over a longer period of time, the bending effect is also observed on the heat sink body. Fig. 9 shows how the heat sink bending is peaking at 20 s (contact fraction minimum). The average sigraflex heat flux value shown in plots is extracted from the thermal simulation; therefore, the loss of contact is not included. A thermally-structural coupled field model needs to be introduced to include the thermal effect of lost contact between graphite and the heat sink. This thermal effect is a concern mainly beause of the tile overheating over multiple NBI pulses. In our case, the recommended resulting dwell times between NBI pulses were doubled to ensure the loss of contact would not cause any overheating during the HST calibration.

Fig. 10 shows the maximal temperature in graphite and heat sink body over time of the 1.5 s of NBI pulse followed by a 1 min cooldown. The Two-way coupled fully coupled model was developed in later stage to uncover the thermal influence of lost contact between graphite and heat sink. The fully coupled model clearly shows how the cooldown rate is affected: the rate of cooldown of the graphite part is lower in the two-way coupled model, confirming the already observed loss of thermal contact dynamic.

3.3. *Structural submodel results*

Fig. 11 shows the maximal principal stress distribution in part of the submodel. The maximal values are found in the graphite corner region, as expected, where the crack initiated. The values of maximal principal stress reach above 76 MPa in 1.5 s of the nominal NBI pulse.

Fig. 12 shows the final results of maximal principal stresses evaluated through submodeling. The scenarios of nominal load, reduced and modulated load are compared. The modulated and the reduced NBI loads show similar resulting stresses, both reaching only about 65 MPa in 1.5 s (compared to 76 MPa for the full nominal load). Graphite is a brittle material; therefore, the strength of the material is defined as a distribution on a wide range of values. The graphite flexural strength limit of 60 MPa (minimum garanteed value) is shown

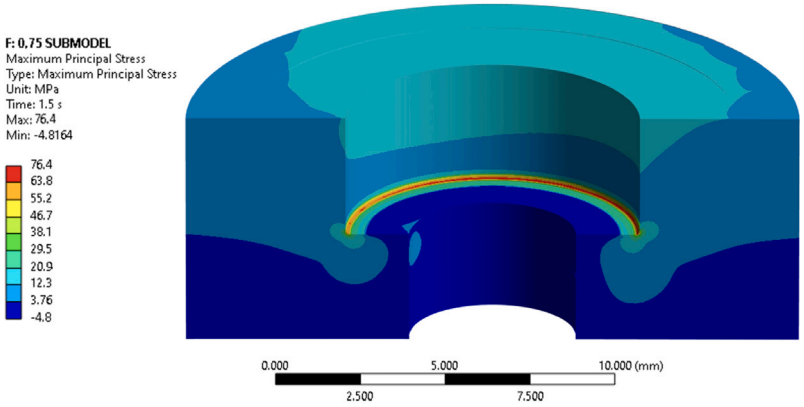

Fig. 11. Maximal principal stress profile in the submodel.

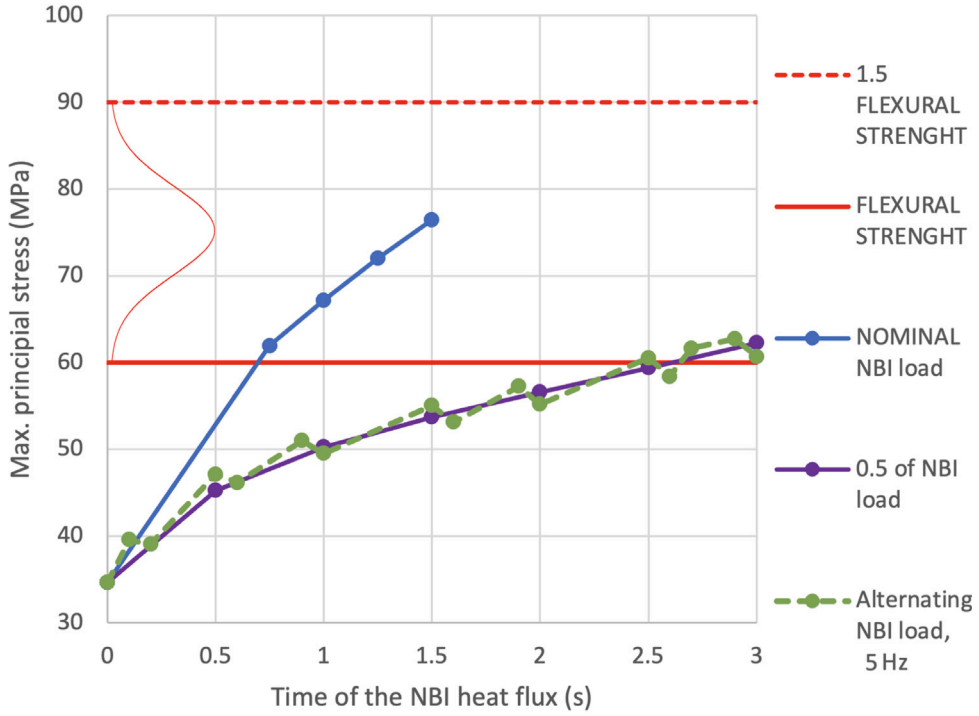

Fig. 12. Maximal principal stress for various scenarios.

along with the 1.5x greater value of stress to estimate the range of the graphite strength. All results found in this range are considered to have some probability of crack initiation and failure. Maximal stresses are reaching the critical value (60 MPa) in only 0.6 s, considering the nominal case. Pulses with modulated heat load lead to about 10% (15 MPa at 1 s of NBI pulse) reduction of the stresses in graphite (comparing the moment when the same average surface temperature is reached in both scenarios), therefore the modulation delays reaching the critical stress region. The average surface temperature is taken as a decisive measure, considering the HST triggering for different load scenarios.

The bolt pretension is found to have a comparable contribution to the bolt force as the thermal load effect, showing the importance to prevent any overtightening of the bolts during the assembly phase. The overtightening of the bolts can have a critical outcome in scenarios where the washers are fully locked just by the pretension, leaving no space for the thermal expansion of materials.

The graphite material properties provided by the manufacturer mention only one-flexural strength value. It is assumed that the manufacturers tend to underestimate the real values of strengths for brittle materials to ensure the certified quality. Having multiple test results with the resulting strengths will allow us to have a more detailed look into the strength distribution. The currently assumed stress distribution is shown as a normal distribution curve in Fig. 12. Evaluating the exact curve required experimental measurements.

The maximal stress region was further examined in the submodel results. For the maximum principal stress in the corner radius (where the maximum value of principal stress occurs), the angle of stress vector was evaluated and compared with the crack initiation angle measurement on the graphite fragments. In theory, the vector of maximal principal stress should be perpendicular to the initial crack direction.

The resulting angles relative to the bolt axis are 40.5° in simulation and 40.2° measured. The simulation results show a strong agreement with the observed crack initiation behavior in the experiments, with results within 1% of the measured values.

4. Conclusions

The destruction of one of the heat shield graphite tiles during OP 2.1 was explained to be a result of high stresses induced by the bending effect of graphite tile under a high temperature gradient. The submodel confirmed that the maximal stress concentrations are found in the area near the bolt holes where the initiation of the crack was found. The exact value of brittle graphite strength cannot be specified by one value but rather a range of values with a probability distribution; therefore, we are not able to accurately predict the onset of damage. Simulation results provided guidance on NBI operation adjustments to prevent further tile destruction in the future W7-X operation. The limit of NBI pulse duration for entering the critical strength region of graphite (> 60 MPa) was specified to be 0.6 s in the case of the nominal load and 2.6 s for the alternating NBI load reduced to half heating power. It was found that the quality of thermal contacts is highly affected by the structural bending of the tile.

The bending effect of graphite (and later the heat sink) largely affects the thermal contact between graphite and the heat sink, reducing the contact surface in peak down to 10% of the area. Contact is present on average in cca 50% of the area for the first few minutes; thus, the total dwell time between pulses should be multiplied by 2 to include this effect. Recommended dwell time considering the loss of contact is 12 min, which was later confirmed by the two way copled calculation.

There is a second negative peak in contact fraction (second loss of contact a few seconds after the first one), caused by the heat sink bending. However the corresponding increase in bolt force and the maximal principal stress in graphite is not significant in comparison with the first peak.

CRediT authorship contribution statement

Vojtěch Smolík: Writing – review & editing, Writing – original draft, Visualization, Validation, Supervision, Software, Resources, Project administration, Methodology, Investigation, Formal analysis, Data curation, Conceptualization. **Mikhail Khokhlov:** Project administration, Methodology, Formal analysis. **Axel Lorenz:** Supervision. **Samuel Lazerson:** Methodology. **Victor Bykov:** Supervision. **Paul McNeely:** Supervision.

Declaration of competing interest

The authors declare the following financial interests/personal relationships which may be considered as potential competing interests: Vojtech Smolik reports writing assistance was provided by Max Planck Institute of Plasma Physics. If there are other authors, they declare that they have no known competing financial interests or personal relationships that could have appeared to influence the work reported in this paper.

Acknowledgments

This work has been carried out within the framework of the EUROfusion Consortium, funded by the European Union via the Euratom Research and Training Programme (Grant Agreement No 101052200 — EUROfusion). Views and opinions expressed are however those of the author(s) only and do not necessarily reflect those of the European Union or the European Commission. Neither the European Union nor the European Commission can be held responsible for them.

Appendix. Material properties

Material Quantity Unit	Graphite R6510 Thermal conductivity [W·m^{-1} ·° C^{-1}]	CuCrZr 2.1293 Thermal conductivity [W·m^{-1} ·° C^{-1}]	Steel 1.4435 Thermal conductivity [W·m^{-1} ·° C^{-1}]
20	128.5	338	13.5
100		342	14.9
200	120.9	350	16.7
300	110.5	360	18.3
400	94.0	372	19.8
500	88.4	387	21.3
600	81.0	404	22.7
700	73.9	423	24.2
800	69.8		25.6
900	63.3		
1000	59.6		
1100	54.9		

Material Quantity Unit	Sigraflex (normal direction) Thermal conductivity [W·m^{-1} ·° C^{-1}]	Sigraflex (in-plane direction) Thermal conductivity [W·m^{-1} ·° C^{-1}]
20	3.0	154
250	2.6	105
500	2.1	82
750	2.1	69
1000	2.1	61
1250	2.1	56
1500	2.1	53
2000	2.1	51

Data availability

Data will be made available on request.

References

[1] N. Rust, et al., W7-X neutral-beam-injection: Selection of the NBI source positions for experiment start-up, Fusion Eng. Des. 86 (6–8) (2011) 728–731, http://dx.doi.org/10.1016/j.fusengdes.2011.03.054.

[2] O. Grulke, et al., Overview of the first Wendelstein 7-X long pulse campaign with fully water-cooled plasma facing components, Nucl. Fusion 64 (11) (2024) 112002, http://dx.doi.org/10.1088/1741-4326/ad2f4d.

[3] X.B. Peng, et al., Thermo-mechanical analysis of Wendelstein 7-X plasma facing components, Fusion Eng. Des. 88 (9–10) (2013) 1727–1730, http://dx.doi.org/10.1016/j.fusengdes.2013.03.056.

[4] R. Schroeder, et al., Safety system of W7-X neutral beam injection heating system, Fusion Eng. Des. 161 (2020) 111922, http://dx.doi.org/10.1016/j.fusengdes.2020.111922.

[5] V. Giannella, et al., LCF assessment on heat shield components of nuclear fusion experiment "Wendelstein 7-X" by critical plane criteria, Procedia Struct. Integr. (2018) 318–331, http://dx.doi.org/10.1016/j.prostr.2017.12.033.

[6] S.A. Lazerson, et al., Modeling and measurement of energetic particle slowing down in wendelstein 7-X, Nucl. Fusion 61 (2021) 096005, http://dx.doi.org/10.1088/1741-4326/ac0771.

[7] J. Fellinger, et al., Overview of fatigue life assessment of baffles in wendelstein 7-X, Fusion Eng. Des. 136 (2018) 292–297, http://dx.doi.org/10.1016/j.fusengdes.2018.02.011.